Materials Advances

ROYAL SOCIETY OF CHEMISTRY

PAPER

View Article Online
View Journal | View Issue

Check for updates

Cite this: *Mater. Adv.*, 2024, 5, 5106

Understanding the impact of silica nanoparticles in cancer cells through physicochemical and biomolecular characterizations†

Asia Saorin, [ad] Alberto Martinez-Serra, [b] Germán Jose Paparoni-Bruzual,[a] Michele Crozzolin, [a] Vincenzo Lombardi,[a] Michele Back, [a] Pietro Riello, [a] Marco P. Monopoli [b] and Flavio Rizzolio *[ac]

Synthetic amorphous silica nanoparticles (SASNs) have emerged as versatile nanomaterials with extensive applications across multiple domains. Their unique physicochemical properties, including controllable size, tuneable surface chemistry, and high stability, have attracted substantial interest for diverse applications, ranging from electronics and materials science to biomedicine. However, the discussion about their toxicity is still open. In this article, we synthesized Stober nanoparticles (SiNPs) and mesoporous silica nanoparticles (MSNs), which consist of SBA-15 and mesocellular foams (MCFs). Their stability in cell culture media (CCM) and consequent protein corona formation were investigated prior to cytotoxicity evaluation. The analysis of the protein corona revealed differences in the relative abundance of proteins related to different sizes of SiNPs and different CCM. The cytotoxicity of the synthesized nanomaterials was evaluated in different cancer cell lines and normal lung fibroblasts. Hemolysis data of SiNPs indicated that smaller nanoparticles (NPs) present in higher numbers per unit of mass were more toxic, but this was not reflected in others cytotoxicity standard tests. The results indicate that long-term exposure of cells to silica-based treatments can significantly affect their viability, with the extent of this effect being related to the characteristics and stability of particles. Therefore, the consideration of these factors is crucial when evaluating the potential applications of NPs in drug delivery or imaging.

Received 29th January 2024,
Accepted 14th April 2024

DOI: 10.1039/d4ma00084f

rsc.li/materials-advances

Introduction

Synthetic amorphous silica nanoparticles (SASNs) are one of the most produced nanoparticles worldwide.[1] SASNs can be categorized into four major categories based on their synthesis: pyrogenic, precipitated, gel-based, and colloidal based.[2] Colloidal silica has been proven to have the potential for biomedical applications, being useful for the development of interesting functional nanoparticles, which can be used for imaging, drug delivery or theranostics.[3–6]

Stober nanoparticles (SiNPs) are colloidal silica particles used for imaging since they show a high control over size, shape and distribution with excellent capacity as host materials for fluorescent probes, which can be both organic and inorganic[4,7–10], with also patented formulation.[11] SiNPs were also proven to be applicable in cancer therapy where they have been used for delivery of chemotherapeutic agents but also gene delivery.[3] Colloidal silica can also be in the form of mesoporous silica nanoparticles (MSNs) characterized by high surface area, which can be easily functionalized. Thanks to this feature, MSNs have been successfully applied for drug delivery of not only small molecules but also DNA and proteins[12] and even reported in patented formulations.[13,14] Among the different types of MSNs, this work focuses on SBA-15 and mesocellular foams (MCFs). SBA-15 has been used for the delivery of proteins and drugs.[15–19] However, small pores determine a delayed release of drugs[20] and an ordered 2D hexagonal structure of SBA materials exhibits steric diffusion hindrance.[21]

[a] *Department of Molecular Sciences and Nanosystems, Ca'Foscari University of Venice, Via Torino 155, Mestre, Italy. E-mail: asia.saorin@unive.it, 877581@stud.unive.it, michele.crozzolin@unive.it, vincenzo.lombardi89@gmail.com, michele.back@unive.it, riellop@unive.it, flavio.rizzolio@unive.it*

[b] *Department of Chemistry, Royal College of Surgeons in Ireland (RCSI), Street 123 St Stephen's Green, Dublin, Ireland. E-mail: amartinezserra@rcsi.ie, marcomonop-oli@rcsi.ie*

[c] *Pathology Unit, Centro di Riferimento Oncologico di Aviano (C.R.O.) IRCCS, Via Franco Gallini 2, Aviano, Italy*

[d] *Immunopathology and Cancer Biomarkers Unit, Centro di Riferimento Oncologico Immunopathology and Cancer Biomarkers Unit, Centro di Riferimento Oncologico di Aviano (CRO), IRCCS, Via Franco Gallini 2, Aviano, Italy*

† Electronic supplementary information (ESI) available. See DOI: https://doi.org/10.1039/d4ma00084f

Therefore, large pores and a non-ordered structure of MCFs could represent a more suitable carrier in certain circumstances and have been exploited in different applications, included cancer treatment.[20–24] SiNPs and some kinds of MSNs such as MCM-41[25,26] are suitable for intravenous injection, while micro-sized MSNs like SBA-15 are mainly considered for oral administration of drugs.[21,27] However, these materials can also be administered as local delivery systems based on subcutaneous or intramuscular injection. This allows the formation of a local depot that can hold high concentrations of the bioactive molecules that are slowly released into the target site.[28–30] Despite these NPs being generally considered biocompatible, their potential effects on the environment and human health are still under debate.[2] Indeed, different factors and experimental designs have to be considered during nanotoxicology experiments such as the synthetic route, aggregation, exposure time, selected cell lines, the presence of serum in the media, toxicity end point detection methods, and doses.[31] The lack of standardization and an insufficient physicochemical characterization of tested NPs have led to disagreement in silica biosafety establishment. For example, in the case of SiNPs, one of the most influencing properties seems to be the size, with smaller nanoparticles (NPs) having higher specific surface area and higher ability to cross the cell membrane.[32–35] However, the results of size-dependent toxicity studies are not completely coherent.[31]

Another factor that has to be considered is that NP surfaces interact with biomolecules once they come in contact with complex biological fluids,[36] forming a cover of biomolecules on top of the NP surface that is known as corona. Mainly formed by proteins, the corona can be divided into three categories, also known as layers: the inner or hard corona (HC), an intermediate layer and the outer or soft corona (SC). Soft corona proteins are weakly bounded and undergo rapid exchanges. In contrast, hard corona proteins are strongly but reversely bound to the surface forming a near-monolayer, which carries the environmental derived identity of the particles.[37,38] These proteins can modify cellular uptake and cellular targeting and decrease the surface energy of NPs lowering their cytotoxicity.[39,40]

The risk assessment evaluation necessitates the application of the most sensitive conditions.[31] Therefore it is necessary to include serum-free conditions in cytotoxicity studies, along with the assessment of interactions between NPs and biomolecules, and the resulting physiological responses of the organism. This approach is also mandated by the European Commission.[41] In the present study, SiNPs of different sizes and MSNs in the form of SBA-15 and MCFs with different pore sizes were considered. Their stability in solution was evaluated, focusing on dispersion in cell culture media (CCM) with and without fetal bovine serum (FBS), which correspond to the *in vitro* tested conditions. Protein corona formation was evaluated in terms of protein amount and composition. Afterwards, effects of elevated NP concentrations (up to 1 mg mL^{-1}) and exposure time on cancer cell lines were evaluated. The selected cell lines correspond to ovarian (OVCAR-3), colon (HCT116) and lung (A549) cancer cell lines and non-cancerous lung fibroblast MRC5. A549 and MRC5 were previously applied in other studies, therefore allow a comparison with the literature. Meanwhile, less attention was given to other cancer cell lines, which were thought the focus of the present study considering that would be the site of their accumulation in drug delivery or imaging applications. Indeed, previous studies focused on the effect of NPs mainly on cell lines of the respiratory system, digestive system, cardiovascular system, nervous epidermis and macrophages.[31] Hemolysis was also evaluated since it is an important parameter that must be considered for intravenous administration of NPs. Indeed, the consequent release of heme proteins is associated with kidney failure in humans,[42] as well as anemia and more serious blood conditions.[43] Moreover, red blood cells (RBCs) have been used since early times as a model for the evaluation of NP damage of the cellular membrane given their high sensitivity to the NP membranolytic effect.[44] Data obtained from the NP characterization allowed the understanding of differences observed for the different particles, confirming the importance of characterization.

Results

NP characterization in different media

The characteristics of the studied SiNPs and MSNs are reported in Table 1, while transmission electron microscopy (TEM) and scanning electron microscope (SEM) images are shown in Fig. 1. SiNPs showed a narrow size distribution, and stable water dispersion with Z potential values of above −30 mV (Table S1, ESI†). However, sample St21 showed a slightly lower water dispersion with a polydispersity index (PDI) value of around 0.2 and the presence of an aggregation peak in the differential centrifugal sedimentation (DCS) plot (Fig. S1, ESI†). On the other hand, the stability of MSN dispersion in water resulted low; indeed, DLS analysis showed PDI values around 0.5 and therefore Z average values are not a good estimation of hydrodynamic diameter (D_h) in water, while DCS showed peaks with a maximum at around 1 μm (Fig. S2, ESI†).

Cell lines considered for the *in vitro* assay required different cell culture media (CCM) for their optimal growth; indeed, MRC5, A549, OVACR-3 and HCT116 respectively are grown in

Table 1 Characteristics of selected SiNPs (obtained by SEM/TEM images and reported as St(Stober)+size) and MSNs (identified basing on sample characteristics, namely SBA-15 and MCF(mesocellular foam)+pore size). As $m^2\ g^{-1}$: specific surface area; TMB/P123: see materials and methods

Sample name	d (nm)	SD	RSD%
St21	21	2	11
St65	65	7	11
St108	108	11	11
St187	187	16	9

Sample name	TMB/P123	Pore size (nm)	As $m^2\ g^{-1}$
SBA-15	0/1	7.3	872 ± 9
MCF-13	0.3/1	13.5	810 ± 7
MCF-22	0.5/1	22.4	933 ± 8

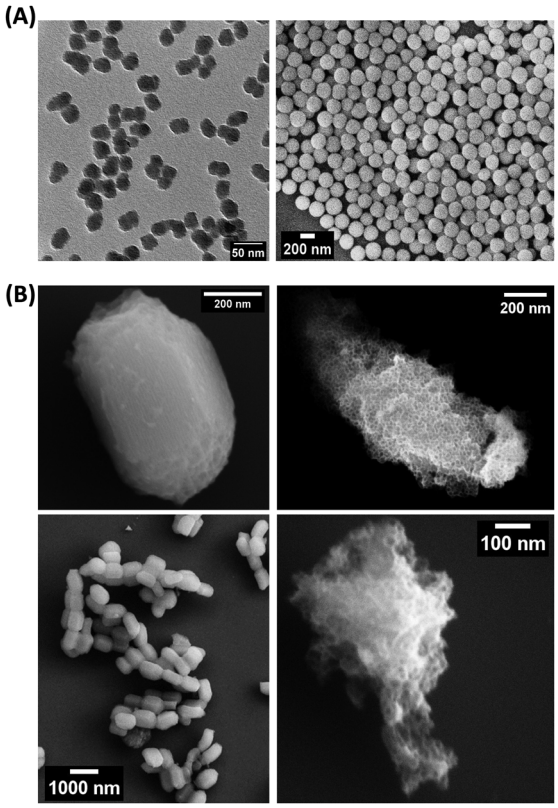

Fig. 1 SEM and TEM images of SiNPs and MSNs. (A) TEM and SEM images of St21 and St187 SiNPs, respectively, on the left and right. (B) SEM images of MSNs: SBA-15 at different magnifications on the right and MCF-22 on the left.

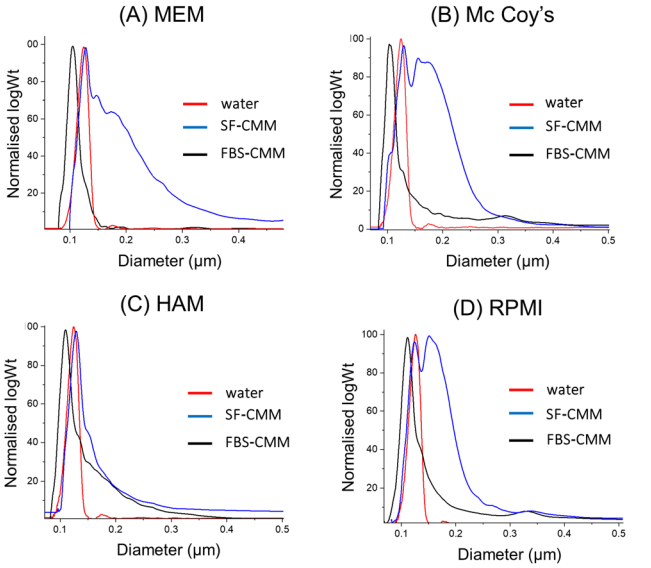

Fig. 2 DCS analysis of St108 dispersed in different CCM (A–D). The *X* axis represents the apparent diameter, while the *Y* axis shows the relative particle weight (log Wt).

the MEM, RPMI 1640, HAM's F12 and McCoy's 5A. In order to evaluate if the size of SiNPs influences the stability in the complex medium environment, RPMI 1640 was selected for the comparison between CCM with 10%FBS (FBS-CCM), serum free CCM (SF-CCM), phosphate buffered saline (PBS) and SC complex. The latter condition was added in order to evaluate the effect of the corona layer without the presence of proteins in the dispersant, and to test the stability of particles in the corona protocol. Moreover, given the observed aggregation of St21 in water, commercial particles with a size of 20 nm (St20Com) were used instead of St21 in order to better evaluate the effect of size on different medium stabilities (in the following sections, St21 SiNPs are also reported since they were the particles applied in cytotoxicity tests).

The formation of protein corona determined a decrease of surface charges (Table S2, ESI†), with *Z* potential SC values being close to the one determined for FBS-CCM (−8.1 mV, FBS-DMEM).[45] However, the presence of protein corona seems to prevent particle aggregation in particular for bigger SiNPs (Fig. S3, ESI†).

In order to evaluate if the stability of SiNPs differs among the different CCM required for the growth of the considered cell lines, dispersions of St108 in HAM's F12, Mc Coy's 5A and MEM as SF-CCM and FBS-CCM were evaluated by DLS and DCS. Particle dispersions in the MEM and Mc Coy's 5A showed similarities with RPMI 1640 with aggregation observed only in the absence of FBS. Differently, HAM's F12 seems to allow good SiNP stability even when the FBS is not present (Fig. 2 and Fig. S4, Table S3, ESI†). Given that aggregation can cause particle precipitation, DLS was used to follow over time the evolution of the number of particles, showing that the number of particles decreased about 50% and takes nearly 20 hours to reach dispersion equilibrium (Fig. S5, ESI†). The stability of MSNs was evaluated by DCS since the low stability of these particles did not allow an accurate measurement by DLS. In analogy with SiNP results, also in this case, the absence of FBS seems to determine lower stability, as it can be seen from the widening of peaks (Fig. S6, ESI†). Moreover, MCFs showed lower stability compared to SBA-15 and MCF-22 and seemed to be less stable than MCF-13, also in the presence of FBS. Given the low general stability, SC samples were not considered given that the protein corona protocol requires the stable dispersion of particles.

Hard corona protein quantification and composition

Quantification of hard corona proteins per unit of silica mass revealed a higher protein content for smaller SiNPs, but after normalization on the surface area the trend is inverted (Fig. 3). Given the discussed instability of MSN dispersions, their protein analysis can estimate protein coverage during the *in vitro* test rather than strictly HC. MCF-22 and SBA-15 showed higher amounts of proteins per unit of silica mass; however, after normalization on the surface area, the difference between MCF-13 and MCF-22 was not significant (Fig. 3).

The HC composition was investigated by SDS–PAGE. SiNPs were initially incubated with 10% FBS diluted in PBS to mimic *in vitro* exposing conditions. Sample St21 showed low band intensities, reasonably as a consequence of its higher

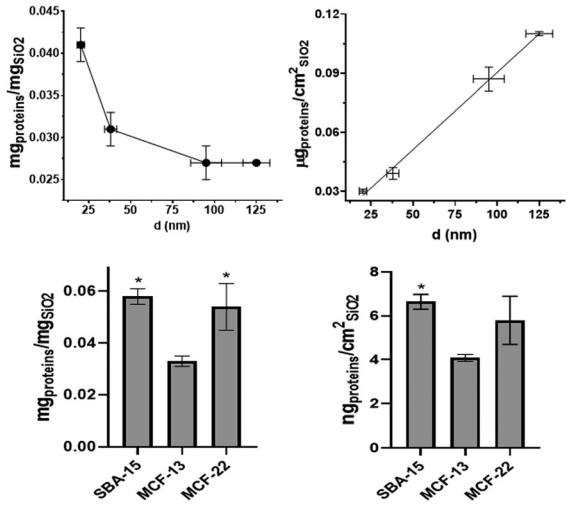

Fig. 3 Protein corona quantification. The protein amount expressed per unit of particle mass (left) and unit of the surface area (right) for SiNPs and below MSNs (Student's t-test was performed *vs.* MCF-13).

aggregation while band intensities of the other samples are in line with quantification data (Fig. 3 and Fig. 4). Looking at the densitometric analysis of different sizes, it seems that proteins with low MWs are more important for smaller particles. Indeed, a protein band at around 30 kDa increases its relative intensity moving to smaller SiNPs. PBS can be used for the dilution of FBS used for the incubation step of the protein corona protocol; however, *in vitro* experiments require CCM. Therefore, in order to evaluate if CCM influence the formation of protein corona and to mimic better *in vitro* experiments, St108 SiNPs were incubated in FBS-CCM. Mc Coy's 5A differs in terms of relative intensities with a significant higher contribution of smaller proteins (30 kDa).

This was also confirmed following the time evolution of the HC composition up to 96 hours (exposure time applied in toxicity tests) where the comparison between McCoy's 5A and RPMI 1640 showed an increment of relative intensities for smaller proteins more pronounced for McCoy's 5A (Fig. 4). The protein profile of MSNs incubated with FBS-Mc Coy's 5A was also evaluated. Comparing MSN profiles with FBS, MSNs clearly selectively concentrate some of the proteins from FBS (Fig. S7, ESI†).

Cytotoxicity

High concentrations of NPs, up to 1 mg mL^{-1}, were applied for the evaluation of hemolysis and cytotoxicity on cancer (OVCAR-3, HCT116, and A549) and normal (MRC5) cell lines maintained in both FBS-CCM and SF-CCM. Moreover, an exposure time of 96 hours was applied considering that tumour would be the therapy target site. In the case of Stöber NPs, hemolysis increases with SiNP concentrations following an exponential plateau curve with the plateau reached at about 0.25 mg mL^{-1}. The hemolysis level reached at plateau increases with the NP size decrement (Fig. 5). However, after normalization on the surface area, larger SiNPs show a higher hemolysis per unit of area (Fig. S8, ESI†). Hemolysis plots of MSNs differ significantly from the ones of SiNPs and reach lower values. SBA-15 shows a linear trend while MCFs do not significantly increase the

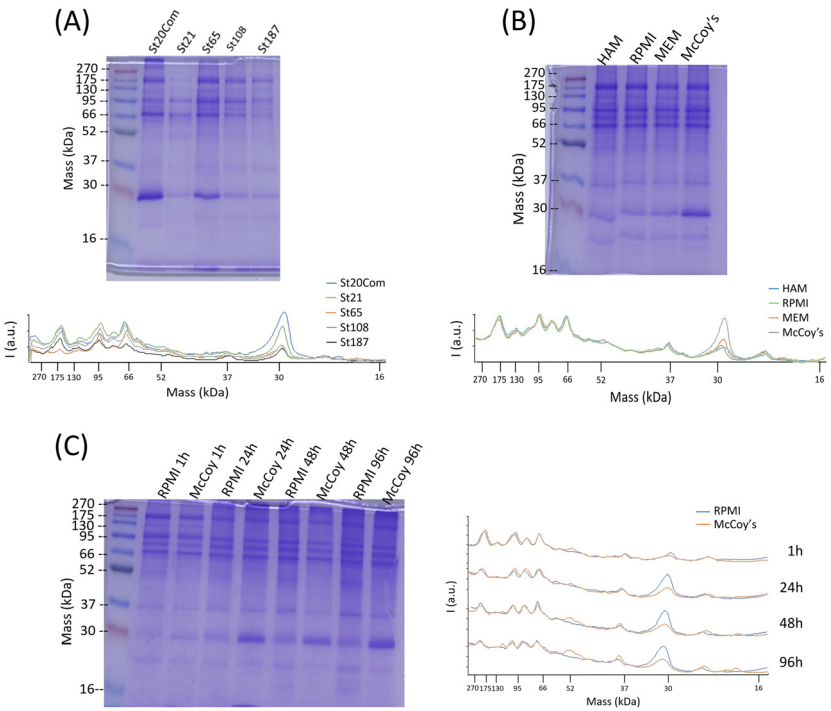

Fig. 4 SDS–PAGE and relative plot of densitometric analysis. (A) Different sizes of SiNPs incubated in 10%FBS with PBS. (B) St108 SiNPs incubated in CCM with 10%FBS. (C) St108 SiNPs incubated with RPMI and Mc Coy's 5A with 10%FBS at different incubation times.

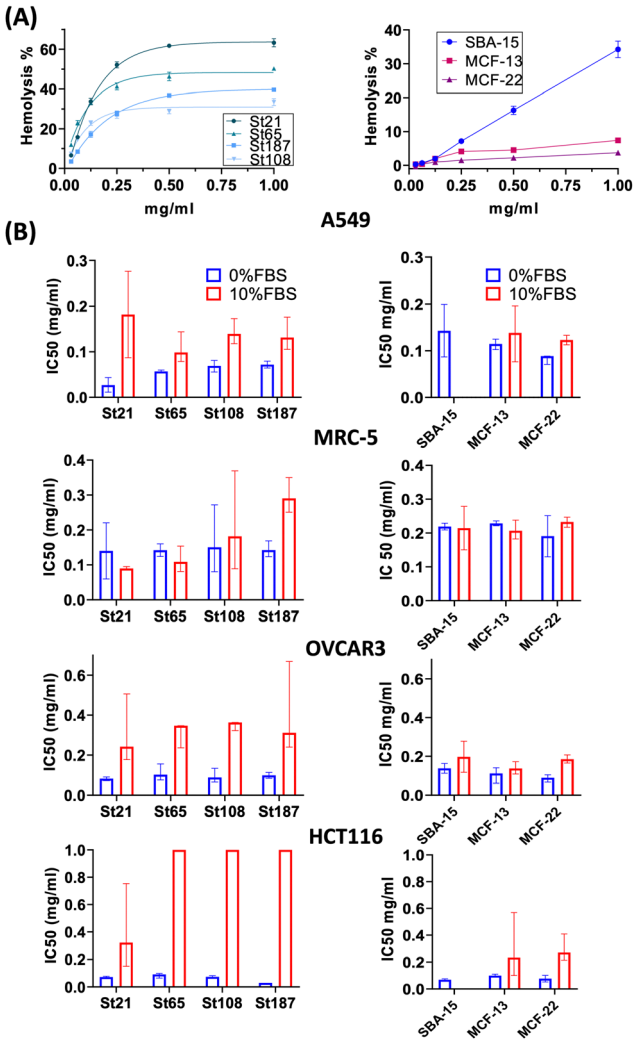

Fig. 5 Hemolysis and cytotoxicity results (IC50). (A) On the left, the plot of hemolysis percentage *vs.* the SiNP concentration fitted by the exponential plateau curve. On the right, the plot of hemolysis percentage *vs.* the MSN concentration. (B) IC50 values of SiNPs and MSNs respectively on the left and on the right (error bars refer to the 95% confidence interval).

hemolysis when their concentrations increase, remaining at values below 10% (Fig. 5). The hemolysis of SBA-15 remains significantly higher than that of MCFs, even after normalization on the surface area (Fig. S8, ESI†). In the presence of FBS, all the cell lines were affected by SiNP treatment after 96 hours of exposure, showing a concentration trend. Viability reduction was more consistent for A549 (Fig. S10, ESI†) and MRC-5 (Fig. S12, ESI†), followed by OVCAR-3 (Fig. S9, ESI†) and finally HCT116, which reported a consistent lower level of cell death (Fig. S11, ESI†). In order to understand if protein corona could be responsible of the different response of HCT116 in presence of FBS, cells were adapted to grow in RPMI 1640 instead of McCoy's5A, indeed the latter correspond to a different protein corona profile. However, viability reduction of HCT116 grown with RPMI 1640 does not differ from the one in McCoy's 5A (Fig. S17, ESI†). Under serum free conditions, a slight change in the morphology of A549 was observed with cells assuming a spherical shape and a decrease of the growth rate, which was also previously reported.[40] All the other cell lines did not reveal obvious alterations in SF-CCM.

Higher differences were visible for HCT116 followed by A549, OVCAR-3 and finally MRC-5 with close IC50 values (Fig. 5). A smaller size corresponds to a higher number of NPs and a higher specific surface area, but only MRC-5 and A549, respectively, with and without the serum, showed a half-maximal inhibitory concentration (IC50) that increases along with the size of the NPs (Fig. 5). MSNs determined a significant reduction in cell viability after 96 hours, in both the presence and the absence of FBS in CCM. However, when FBS was added, the concentration effect was not so clear in particular for SBA-15. This did not allow the calculation of the IC50 value (Fig. 5) and revealed lower cytotoxicity of SBA-15 than MCFs. Indeed, FBS-CCM results show a slight trend of increasing toxicity moving from SBA-15 to MCF-22 and as last MCF-13. In SF-CCM, all MSNs determined an increase in cell mortality associated with the increase of particle concentrations (Fig. S13–S16, ESI†). Moreover, the removal of FBS determined an increase in cytotoxicity, which was less significant in the case of OVCAR-3 and MRC-5, with the latter showing close IC50 values, in analogy with SiNP results. Apoptosis is frequently reported as the cell death pathway associated with SiNP cell exposure.[46–49] Therefore, with the aim of understanding if apoptosis was responsible for cell mortality observed in the current experimental settings, caspase 3/7 were monitored at different time points up to 24 hours in MRC-5 and A549.

Monitoring caspases in FBS-CCM and SF-CCM was particularly interesting for MRC5, which seem to be less affected by serum removal. A549 cell lines were used as a comparison given that they are derived from the same organ. An earlier and more consistent activation of apoptosis was revealed in SF-CCM, while in the presence of FBS activation was modest and almost limited to 24 hours of exposure (Fig. 6). Comparing MRC-5 and A549 in SF-CCM, A549 showed a more significant activation of caspases at 6 *vs.* 24 hours for the majority of tested silica particles (St21, St108, St187, and SBA-15). Differently, MRC-5 seems to have a higher activation of caspases at 24 hours (St21, St108, St187, SBA-15, and MCF-13). A difference in the interaction between MRC-5 and silica particles was also determined by samples' microscope inspection, which revealed that fibroblasts tended to gather particles during 96 hours of incubation. This was particularly evident in the case of serum free conditions and MCFs, probably due to their low stability in solution (Fig. S18, ESI†).

Discussion

SiNP dispersions in water were stable differently from MSN ones, while in CCM higher stability was achieved in the presence of FBS, in particular for big SiNPs. In the absence of protein corona, the aggregation of SiNPs in CCM and PBS derives from the ionic strength of the solution that screens the negative repulsive charge of SiNPs, which is indeed

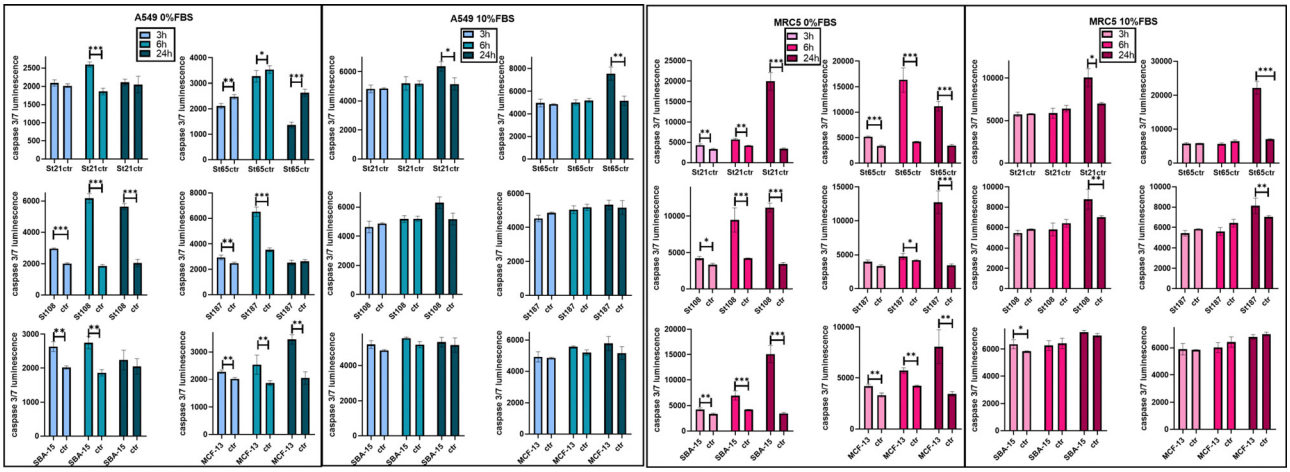

Fig. 6 Activation of apoptosis for MRC-5 and A549 exposed to SiNPs and MSNs. Bar plots of caspase 3/7 luminescence intensities for 3,6 and 24 hours of exposure to 0.25 mg mL^{-1} of particles in SF-CCM (0% FBS) and FBS-CCM (10% FBS).

confirmed by the decrease of the *Z* potential value. While the stabilization deriving from the presence of protein corona probably is achieved from steric repulsions.[45] Aggregation could be followed by the precipitation of the aggregates, which was proven to be of about 50% of total particles in SF-CCM measure. This result agrees with an *in vitro* sedimentation, diffusion and dosimetry (ISDD) model.[50] The ISDD model also establishes that microsphere could reach 100% of precipitation both in water and in FBS-CCM within two hours. MSNs probably share a similar precipitation rate or even faster considering their DLS analysis. DCS revealed that MCFs are less stable than SBA-15, which can be attributed to the loss of the controlled shape. This information about the stability of NPs in *in vitro* settings was fundamental during the evaluation of cytotoxicity results, confirming the importance of this characterization and the requirement of orthogonal techniques. Quantification of hard protein corona of SiNPs revealed that larger nanoparticles showed more adsorbed proteins per surface unit. With regard to gold NPs, it has been proposed that larger NPs are seen by proteins as flat surfaces which lead to a greater tendency to modify their structure to attach NP to surfaces. Surface-driven protein conformational changes allows to cover completely the NP surface since the stabilization of the first layer of proteins acts as a nucleation centre, stabilizing the depositions of new ones.[51] Therefore, this effect could be responsible for the higher protein coverage of larger NPs. However, SiNPs have a larger tendency toward aggregation in complex media compared to gold NPs, so higher aggregation of smaller NPs (confirmed in the present study) could reduce protein adsorption per unit of area since the exposed area is overestimated.[52] The low stability in FBS-CCM can also be responsible for the lower loading of protein per unit of area of MCFs than SBA-15.

The overall results derived from SDS–PAGE experiments on the SiNP protein corona indicate that protein intensities are influenced by SiNP sizes and dispersants. Indeed, small NPs present higher relative abundance of small proteins, which could derive from the limited protein rearrangement that can be particularly important for large proteins.

SiNP hemolysis follows an exponential plateau curve with a plateau value in line with a previous study.[53] The percentage of hemolysis reached at plateau increases with the decrease of the NP size, probably due to the higher number of NPs and specific surface area corresponding to smaller NPs. The hemoglobin absorbance value at 0.5 mg mL^{-1} was normalized by surface area revealing that larger particles have higher hemolysis per unit of area. This may derive from the lower surface curvature corresponding to larger NPs, since the binding energy between NPs and membranes increases with the decrease of curvature.[53] With regard to MSNs, SBA-15 showed higher hemolysis with an almost linear concentration trend. SBA-15 is the most stable MSNs; thus, it might have a higher time of contact with RBCs determining higher values of hemolysis and concentration effects. For MCFs, larger pores corresponded to lower hemolysis since the effective surface area of contact is lower.

Cytotoxicity results showed that in the presence of serum, HCT116 cell lines are highly resistant to NP treatment, and this is not a consequence of their different protein corona profiles. However, the difference observed in terms of the relative abundance of proteins in HC, could be determined by the high amount of glucose present in Mc Coy's 5A. Indeed, it is the only considered media being high glucose (3000 mg L^{-1}) and a previous study,which focused on the effect of different glucose contents in human plasma on protein corona compositions of liposomes, revealed that different concentrations of glucose affected the relative protein abundance. This is probably due to glucose selective interactions with specific proteins or glucose action as a linker between proteins and NP functional groups.[54] However, this increase of NP toxicity under serum free condition was less consistent for MRC-5. Differently from hemolysis, only MRC-5 and A549, respectively in FBS-CCM and SF-CCM, showed IC50 values which tend to increase along with the size of the NPs, *i.e.* with a decreasing number of NPs. It is interesting to notice that HAM F12 was the only CCM associated with

good NP stability in the absence of FBS. Therefore, size dependency under serum free conditions could be masked by particle aggregation, which does not occur or occur in lower levels in the case of HAM F12, allowing the size effect to be revealed. The higher stability in HAM F12 could derive from different compositions in terms of salts. Indeed, HAM F12 is the only considered medium that does not share a common salt composition (Table S4, ESI†). In the case of MSNs, the cytotoxicity test performed in FBS-CCM shows a slight trend of increasing toxicity moving from SBA-15 to MCF-22 and finally MCF-13. This is in line with hemolysis; indeed, SBA-15 has higher stability in solution than MCFs and therefore they have a higher time of contact with RBCs and lower with adherent cells. MCFs, instead, have low stability in solution which determined lower hemolysis and higher cytotoxicity. Moreover, MCF-13 have smaller pores which corresponds to a wider active area of contact with cells. Therefore, MCF-13 presented both higher hemolysis and cytotoxicity than MCF-22. Another factor that might contribute to increment MCF-13 effects on cells is the extent of protein coverage since they showed the lower amount of protein per unit of mass and area. Apoptosis was confirmed for A549 and MRC5 even if with different activation times and more consistent in the absence of serum. A previous work analyzed lower concentration of similar sizes of SiNPs on MRC-5 revealing that particles induced autophagy but not apoptosis.[55] Therefore, increasing the SiNP concentration might shift from autophagy to apoptosis. Overall, the cytotoxicity results confirm that MRC-5 responds differently to serum free conditions, and this translates into a less acute response to silica exposure. The different behavior of MRC-5 might be in part attributed to the tendency of MRC-5 to gather NP aggregates. This behavior was also determined in the other work with SiNPs[56] but also for other particles.[57] Fibroblasts are structural cells of connective tissues with a role in the deposition of extracellular matrix (ECM) components (collagens I, II, and V) and formation of basement membranes by secreting type IV collagen and laminin.[58] The absence of FBS is known to increase the cytotoxicity of NPs since when bare NPs reach cells, they use cellular component to form protein corona causing membrane and cell damage associated with a high NPs internalization.[40] Therefore, it might be that normal fibroblasts are less affected by serum free silica treatment given that particles can find other protein sources, which although facilitate their accumulation as aggregates on cell membranes.

Experimental

Piston pump assisted synthesis of Stöber SiNPs

In the synthesis of Stöber NPs, a piston pump was used for the dropping of an ethanolic TEOS (Sigma Aldrich, 131903) solution 1.34 M at 1 milliliter per minute into a round flask containing ethanol (Sigma Aldrich, V001229), water (Milli-Q®,Millipak® 0.22 μm) and ammonia (Merck, 1.05423) with a total final volume of 50 mL and maintained at 30 °C. The reaction was maintained overnight and then NPs were separated and washed three times with ethanol using an ultracentrifuge Sorvall™ WX (Thermo Scientific, Waltham, Massachusetts). Finally, NPs were dried at 60 °C overnight. Commercial silica NPs of 20 nm in diameter (PSI-0.02, Kisker Biotech GmbH (Germany)) were used as the reference (reported as St20Com).

Synthesis of MSNs

In the synthesis of SBA-15, triblock copolymer Pluronic P123 (Sigma Aldrich, 435465) was used as the template. Initially, 4 g of P123 was dissolved in 116.5 mL of aqueous HCl 2 M (Merck Millipore, 100317) and transferred into a double jacketed round-bottom flask containing 30 mL of water and equilibrate to 35 °C. Then, 9 mL of TEOS was dropped under stirring using a dropping funnel can and the reaction was maintained for 20 hours. Then, the solution was added into a closed container and heated at 90 °C in an oven for 24 hours (BINDER GmbH, Tuttlingen, Germany). Then, samples were filtered, washed with water and dried at 60 °C in the oven. Finally, the samples were calcined in AAF 1100 (Carbolite Gero, Hope, UK) under air at 550 °C for 6 h. MCFs were obtained by the addition of 1,3,5-trimethylbenzene (Sigma Aldrich, 442236) as the swelling agent at TMB/P123 ratios equal to 0.3 and 0.5.

SEM and TEM analyses

The size and morphology determination of NPs were carried out with a Carl Zeiss Sigma VP field emission scanning electron microscope (FE-SEM) (ZEISS, Oberkochen, Germany) or using an FEI Tecnai G2 transmission electron microscope operating at 100 kV (Hillsboro, Oregon, US) equipped with a Veleta digital camera (Olympus Soft Imaging System). Image processing was carried out using the ImageJ (1.52a) software (National Institutes of Health, Bethesda, Maryland).

DLS and *Z* potential

DLS was used for the measurement of Dh and PDI of NPs in water, PBS (P4417, Sigma Aldrich), SF-CCM (ThermoFisher Gibco, Waltham, Massachusetts), and FBS-CCM after incubation for 1 h at 37 °C and the NP–SC complex in PBS (see "Incubation and corona isolation" section). Samples for DLS were prepared at 0.4 mg mL^{-1} and then diluted for measurements in a concentration range between 50 and 100 μg mL^{-1}. Dispersants were 0.22 μm filtered before NP addition. For each sample, at least three measures were obtained, each one composed of 12 subsequent runs. Dh and PDI correspond to the *Z*-average value, but in the case of FBS-CCM which presents peaks at around 10 nm deriving from proteins, Dh was obtained from the NP peak and PDI estimated from the standard deviation of the peak. CCM viscosity values at 25 °C were estimated based on the glucose content and presence of FBS.[59,60,] Refractive index was considered constant and equal to 1.34564. DLS was also applied for the evaluation of the time course stability of SiNP (g) dispersion in CCM (Mc Coy's 5A). The selected concentration was equal to 0.25 mg mL^{-1} since the purpose was to evaluate the stability at high concentrations, but sample needs also to fit the requirement of DLS analysis.

Particle counting (PC), size and PDI values were determined up to 60 hours at 25 °C. Measurements were performed using a zetasizer nanoparticle analyzer (Malvern Panalytical, Malvern, UK).

DCS

Gradient was realized with aqueous sucrose solutions with concentrations ranging from 2% to 8%, a maximum measured size of 5 μm with a centrifugal force equal to 18 000 rpm. A calibration standard was run prior to each sample measure, and 100 μL of samples with a concentration of minimum 0.5 mg mL^{-1} were injected, with smaller NPs requiring higher concentrations. Gradient was replaced after injection of samples in CCM in order to maintain its integrity. Measures were performed using a CPS disc centrifuge (CPS Instruments, Oosterhout, The Netherlands). Plots are reported as the logarithm of the weight (log Wt).

Surface area and pore size measurements

Nitrogen adsorption–desorption isotherms were measured at a liquid nitrogen temperature using a Micrometrics ASAP 2010 system (Microtrac Retsch GmbH, HAan, Germany). Each sample was degassed at 130 °C overnight before the measurements. The Brunauer–Emmett–Teller (BET) equation was used to calculate the specific surface area from the adsorption data and the Barrett–Joyner–Halenda (BJH) model was used to estimate the pore-size distribution from the adsorption branches of the isotherms. In the case of SiNPs, five samples were subjected to surface areas measured by BET and by theoretical calculations,[50] proving that theoretical values are a good approximation of the surface area. Therefore, for the other SiNPs, surface areas were calculated.

Incubation and corona isolation

SiNPs were incubated under determined conditions for different times (from 1 to 96 h) at 37 °C by mixing at 300 rpm using a thermal shake lite (Avantor, Radnor, Pennsylvania, USA) in low binding Eppendorf® tubes. When incubation was completed, the samples were centrifuged (18 000*g*, 15 minutes, 15 °C) using a Micro Star 17R (Avantor, Radnor, Pennsylvania, USA). The supernatants were removed, and the pellets were redispersed in PBS by mixing with the pipette (SC). To obtain the SiNP–HC complex, samples were washed three additional times followed by centrifugation and redispersion. Finally, the pellets were transferred into a new Eppendorf® tube for the following analysis.[61]

Protein corona quantification using the Bradford protein assay

The method was adapted from the one reported by Partikel *et al.*,[62] using a photometric method developed by Bradford *et al.*[63] Particles were subjected to the hard protein corona protocol (1.5 mg in 1 mL of Mc Coy's 5A). The obtained pellets were dispersed in water and lyophilized. Then, 250 μL of NaOH 0.2 M (S5881, Sigma Aldrich) was added to each pellet and incubated for 20 minutes at 60 °C under agitation (1200 rpm) using a thermal shake lite (Avantor, Radnor, Pennsylvania, USA). For SiNPs, 200 μL of samples were mixed with 20 μL of H_3PO_4 5 M (345245, Sigma Aldrich), 580 μL of water and 200 μL of the protein dye (Bio-rad protein assay). Meanwhile, in the case of MSNs, 50 μL of samples were mixed with 5 μL of H_3PO_4 5 M, 745 μL of water and 200 μL of the protein dye. After 15 minutes from the addition of the dye, the absorbance was read at 595 nm with the reference at 350 nm using a plate reader Synergy H1 (Agilent, Santa Clara, California). Calibration curves were obtained from solutions of bovine serum albumin (BSA) (05479, Sigma Aldrich) subjected to the same sample preparation. The limit of detection (LOD), limit of quantification (LOQ) and linearity limit were established. All the samples were measured in triplicates.

SDS–PAGE

SDS-PAGE was carried out to visualize differences in the protein corona gel bands across the samples. SiNPs at a concentration of 0.4 mg mL^{-1} or 0.2 mg mL^{-1} in the case of 20 nm samples (to avoid the excess of protein loading) were dispersed in the specified media and subjected to the HC-protocol. Immediately after NP-HC isolation, the pellets were then dispersed in 12 μL of water and 6 μL of 3× loading buffer (New England Biolabs,7722S) with 0.1 M dithiothreitol (DTT) (New England Biolabs,7016L), heated for 5 minutes at 95 °C, then loaded with 10% of acrylamide gels (15 uL) along with a protein ladder (PrimeStep™ Prestained Broad Range Protein Ladder, BioLegend, 773301). SDS-PAGE was run at 120 V in the presence of running buffer (glycine (Sigma, G8898), SDS, Tris). After the gel run, protein bands were visualized by Coomassie brilliant blue staining (Imperial Protein Stain, Thermo Fisher, 24617). Gel images were processed by GelAnalyzer 19.1 (**https://www.gelanalyzer.com**, created by Istvan Lazar Jr., PhD and Istvan Lazar Sr., PhD, CSc). FBS and MSN samples were run with precast gels 4–20% of acrylamide (GenScript, M42012). All the experiments were performed in duplicates.

RBC hemolysis

The method was adapted from the one reported by Yu *et al.*[53] Red blood cells were obtained from a donor at the biobank of National Cancer Institute of CRO-Aviano under the informed consent. 80 μL of erythrocytes/D-PBS (from 4 mL of blood) were added to 320 μL of D-PBS containing silica particles with a concentration from 1 mg mL^{-1} to 31.3 μg mL^{-1} obtained by 1 : 2 serial dilution. Positive and negative controls were obtained by the addition of 80 μL of RBC solution to 320 μL of water and D-PBS. Solutions were maintained at room temperature for 4 hours under rotation of 30° obtained by PS-M3D (Grant Instruments, Cambridgeshire, UK). Hemoglobin release was quantified by the absorbance measure at 577 nm with the reference at 655 nm using a plate reader Synergy H1 (Agilent, Santa Clara, California). Positive and negative controls were also used for determining the LOQ, LOD and linearity. Each condition was tested on biological triplicates (RBCs obtained from the same donor) and for each biological sample technical triplicates were obtained, leading to the final average of 9 values. Hemolysis has been reported as the percentage calculated on positive and negative controls.

Cell cultures

Selected cell lines were A2780 (Sigma Inc., St. Louis, MO, USA), HCT116, A549, and MRC-5 (all the three obtained from American Type Culture Collection) which respectively have been cultured using RPMI 1640, McCoy's 5A, HAM's F12 and the MEM with EARLE's salts (ThermoFisher Gibco, Waltham, Massachusetts). CCM were supplemented with 10% v/v FBS (Microtech, Napoli, Italy) and penicillin–streptomycin 1% (Merck, P4333). FBS was inactivated by heat treatment at 56 °C for 30 minutes. Cell lines were also adapted to growth under low serum conditions by gradually decreasing the amount of FBS added to the media. Cells were maintained at a minimum concentration of 1% of FBS which did not determine visible alteration in their morphology. Experiments in SF-CCM were performed using cells adapted at 1% FBS and SF-CCM were supplemented with insulin-transferrin-selenium (ITS-G) (Thermo Fisher Gibco, 41400045) and human epidermal growth factor (h-EGF) (Thermo Fisher PeproTech, AF-100-15). Cell cultures were maintained at 37 °C in a humidified atmosphere containing 5% CO_2 according to the supplier. Cells were grown in a cell culture flask (Falcon® 75 cm^2, 353136, Corning) and cell splitting was performed at 70–80% of confluency using trypsin (Thermo Fisher Gibco, 25200072) and a seeding density of 2×10^{-4} cm^{-2}. Cells used in experiments correspond to passage number lower than 20. The morphology and growth of cells were daily checked using the microscope to ensure cell health. Cells were routinely tested to be mycoplasma free (Lonza MycoAlert® PLUS Kit – Mycoplasma Detection Kit).

Cell viability assay (IC50)

Cells were seeded in 96-wells plates (Sarsted, 83.3925) and incubated for 24 h prior to the treatment with SiNPs and MSNs at concentrations ranging from 1 mg mL^{-1} to 31.3 μg mL^{-1} reached by a serial dilution (1 : 2). Serial dilutions were performed in CCM, with highest concentration solutions obtained by probe sonication (VC-50 Vibra Cell Ultrasonic Processor, Sonics & Materials Inc., Newtown, Connecticut, US) dissolution of dry nanoparticles (30 seconds, ice cooled).[64] Cells were seeded in different numbers based on the cell line and the presence of FBS. In the presence of FBS, the seeding density was equal to 1×10^{-3} per well and 4×10^{3} per well respectively for cancerous cell lines and MRC-5. In the absence of FBS, the seeding density was equal to 5×10^{3} per well; indeed, it has been optimized to obtain around 70–80% of confluency after 96 hours. The cell viability was assessed after 96 h of exposure time using the CellTiter-Glo® Luminescence assay (Promega, WI, USA), using a plate reader Synergy H1 (Agilent, Santa Clara, California). SiNPs were added to CCM and luminescence was read revealing no interference of SiNPs in the assay. Negative controls were used to obtain normalized viability values. IC50 values were calculated with Graph Pad Prism 4.0 (Graph Pad Software Corporation, San Diego, CA, USA). Each experiment consists of biological triplicates and reported IC50 values were obtained by their average ± 95% confidence interval (CI).

Caspases 3/7

Cells were seeded at a density of 5×10^{-3} per well in 96 wells plate. After 24 hours, cells were treated with 0.25 mg mL^{-1} NPs in CCM. Caspases 3/7 were determined at different exposure times using a Caspase-Glo® 3/7 Assay System (Promega, Madison, Wisconsin, USA). The luminescence signal was read using a plate reader Synergy H1 system (Agilent, Santa Clara, California). Reported values refer to the average of biological triplicates.

Statistics

Data are reported as average ± standard deviation (SD), if not differently specified on the correspondent materials and methods section. Comparisons are performed by Student's *t*-test and differences among the investigated groups were considered significant for $p < 0.05$. Different significance levels were reported as follows: * for $0.05 > p > 0.01$; ** for $0.01 > p > 0.001$; *** for $0.001 > p > 0$. Analysis and graphing are performed with Graph Pad Prism 4.0 (Graph Pad Software Corporation, San Diego, CA, USA) and Origin (OriginLab corporation, Northampton, Massachusetts).

Conclusions

Stability investigations revealed that SiNPs, even if highly stable in water solution, decrease their stability in complex media. However, in particular for larger sizes, the presence of protein corona increases particle stability. Moreover, the analysis of protein corona reveals differences not in terms of composition but in terms of the relative abundance of proteins related to different sizes of SiNPs and CCM. MSNs showed in general low stability in solution, in particular in the form of MCF. For all the cancer cell lines, the removal of the serum from CCM determined an increment of toxicity, while normal lung fibroblasts reported a higher resistance under serum free conditions. This might derive from the tendency of MRC-5 to accumulate particle aggregates on their membranes. A clear trend of size toxicity was not evident other than MRC-5 and A549 respectively in the presence and absence of FBS. However, this trend was visible for hemolysis, which reach higher percentages for smaller nanoparticles. MSNs showed the cytotoxicity and hemolysis trend, which can be explained considering the higher stability in solution of SBA-15 and the pore size. Overall, these results seem to indicate that long time of exposure to silica treatment significantly affects cell viability even if different cell lines showed different responses, and this should be considered for silica application in drug delivery or imaging. Moreover, data on dispersion stability and protein coverage have been proven to be important to understand cytotoxicity responses. Therefore, characterization of particle stability in complex media is a fundamental parameter that has to be considered.

Author contributions

A. S., A. M. S., and G. J. P. B. were involved in the conceptualization, experimental data and writing; M. C., M. B., and

V. L. participated in the investigation, formal analysis and data curation; F. R., M. P. M., and P. R. contributed to the conceptualization and review and editing; F. R. and M. P. M. were involved in funding acquisition. All authors read and approved the final manuscript.

Conflicts of interest

There are no conflicts to declare.

Acknowledgements

A. S., A. M. S. and M. P. M. acknowledge the support from the European Union's Research and Innovation Programmes under grant agreement no. 952924 (SUNSHINE) and 101092901 (POTENTIAL). A. S. acknowledges the support from Italian Ministry of Health, Ricerca Corrente.

References

1 J. G. Croissant, K. S. Butler, J. I. Zink and C. J. Brinker, Synthetic amorphous silica nanoparticles: toxicity, biomedical and environmental implications, *Nat. Rev. Mater.*, 2020, **5**, 886–909.
2 B. Giese, F. Klaessig, B. Park, R. Kaegi, M. Steinfeldt, H. Wigger, A. von Gleich and F. Gottschalk, Risks, release and concentrations of engineered nanomaterial in the environment, *Sci. Rep.*, 2018, **8**, 1565.
3 V. Gubala, G. Giovannini, F. Kunc, M. P. Monopoli and C. J. Moore, Dye-doped silica nanoparticles: synthesis, surface chemistry and bioapplications, *Cancer Nanotechnol.*, 2020, **11**, 1–43.
4 C. Mochizuki, J. Nakamura and M. Nakamura, Development of non-porous silica nanoparticles towards cancer phototheranostics, *Biomedicines*, 2021, **9**, 73.
5 K. B. Seljak, P. Kocbek and M. Gašperlin, Mesoporous silica nanoparticles as delivery carriers: An overview of drug loading techniques, *J. Drug Delivery Sci. Technol.*, 2020, **59**, 101906.
6 M. Vallet-Regí, Nanostructured mesoporous silica matrices in nanomedicine, *J. Intern. Med.*, 2010, **267**, 22–43.
7 A. Burns, H. Ow and U. Wiesner, Fluorescent core–shell silica nanoparticles: towards "Lab on a Particle" architectures for nanobiotechnology, *Chem. Soc. Rev.*, 2006, **35**, 1028–1042.
8 K. Ma, C. Mendoza, M. Hanson, U. Werner-Zwanziger, J. Zwanziger and U. Wiesner, Control of ultrasmall sub-10 nm ligand-functionalized fluorescent core–shell silica nanoparticle growth in water, *Chem. Mater.*, 2015, **27**, 4119–4133.
9 E. Phillips, O. Penate-Medina, P. B. Zanzonico, R. D. Carvajal, P. Mohan, Y. Ye, J. Humm, M. Gönen, H. Kalaigian and H. Schöder, Clinical translation of an ultrasmall inorganic optical-PET imaging nanoparticle probe, *Sci. Transl. Med.*, 2014, **6**, 260ra149.
10 B. Quan, K. Choi, Y.-H. Kim, K. W. Kang and D. S. Chung, Near infrared dye indocyanine green doped silica nanoparticles for biological imaging, *Talanta*, 2012, **99**, 387–393.
11 M. S. Bradbury, U. Wiesner, O. P. Medina, A. Burns, J. S. Lewis and S. M. Larson, *Multimodal silica-based nanoparticles*, 2020.
12 Z. Li, J. C. Barnes, A. Bosoy, J. F. Stoddart and J. I. Zink, Mesoporous silica nanoparticles in biomedical applications, *Chem. Soc. Rev.*, 2012, **41**, 2590–2605.
13 H. W. H. Chan, C.-Y. Mou, C.-H. Wu, S.-H. Wu, Y.-P. Chen and R.-L. Zhang, *Drug delivery by pore-modified mesoporous silica nanoparticles*, 2021.
14 M. Liong, J. Lu, F. Tamanoi, J. I. Zink and A. E. Nel, *Mesoporous silica nanoparticles for biomedical applications*, 2020.
15 T. M. Albayati, I. K. Salih and H. F. Alazzawi, Synthesis and characterization of a modified surface of SBA-15 mesoporous silica for a chloramphenicol drug delivery system, *Heliyon*, 2019, 5.
16 Z. Bahrami, A. Badiei and F. Atyabi, Surface functionalization of SBA-15 nanorods for anticancer drug delivery, *Chem. Eng. Res. Des.*, 2014, **92**, 1296–1303.
17 D. Gkiliopoulos, I. Tsamesidis, A. Theocharidou, G. K. Pouroutzidou, E. Christodoulou, E. Stalika, K. Xanthopoulos, D. Bikiaris, K. Triantafyllidis and E. Kontonasaki, SBA-15 mesoporous silica as delivery vehicle for rhBMP-2 bone morphogenic protein for dental applications, *Nanomaterials*, 2022, **12**, 822.
18 T. Krajnović, D. Maksimović-Ivanić, S. Mijatović, D. Drača, K. Wolf, D. Edeler, L. A. Wessjohann and G. N. Kaluđerović, Drug delivery system for emodin based on mesoporous silica SBA-15, *Nanomaterials*, 2018, **8**, 322.
19 B. Malfait, N. T. Correia, C. Ciotonea, J. Dhainaut, J.-P. Dacquin, S. Royer, N. Tabary, Y. Guinet and A. Hédoux, Manipulating the physical states of confined ibuprofen in SBA-15 based drug delivery systems obtained by solid-state loading: Impact of the loading degree, *J. Chem. Phys.*, 2020, 153.
20 T. Liu, K. Wang, M. Jiang and L. Wan, Interactions between mesocellular foam silica carriers and model drugs constructed by central composite design, *Colloids Surf., B*, 2019, **180**, 221–228.
21 Y. Zhang, J. Zhang, T. Jiang and S. Wang, Inclusion of the poorly water-soluble drug simvastatin in mesocellular foam nanoparticles: drug loading and release properties, *Int. J. Pharm.*, 2011, **410**, 118–124.
22 B. R. Jermy, V. Ravinayagam, S. Akhtar, W. Alamoudi, N. A. Alhamed and A. Baykal, Magnetic mesocellular foam functionalized by curcumin for potential multifunctional therapeutics, *J. Supercond. Novel Magn.*, 2019, **32**, 2077–2090.
23 A. Maleki and M. Hamidi, Dissolution enhancement of a model poorly water-soluble drug, atorvastatin, with ordered mesoporous silica: comparison of MSF with SBA-15 as drug carriers, *Expert Opin. Drug Delivery*, 2016, **13**, 171–181.
24 J. L. Sánchez-Orozco, B. Puente-Urbina, J. A. Mercado-Silva and H. I. Meléndez-Ortiz, β-Cyclodextrin-functionalized

mesocellular silica foams as nanocarriers of doxorubicin, *J. Solid State Chem.*, 2020, **292**, 121728.

25 V. Mamaeva, C. Sahlgren and M. Lindén, Mesoporous silica nanoparticles in medicine—Recent advances, *Adv. Drug Delivery Rev.*, 2013, **65**, 689–702.

26 I. I. Slowing, J. L. Vivero-Escoto, C.-W. Wu and V. S.-Y. Lin, Mesoporous silica nanoparticles as controlled release drug delivery and gene transfection carriers, *Adv. Drug Delivery Rev.*, 2008, **60**, 1278–1288.

27 A. Dadej, A. Woźniak-Braszak, P. Bilski, H. Piotrowska-Kempisty, M. Józkowiak, M. Geszke-Moritz, M. Moritz, D. Dadej and A. Jelińska, Modification of the release of poorly soluble sulindac with the APTES-modified SBA-15 mesoporous silica, *Pharmaceutics*, 2021, **13**, 1693.

28 Y. Choi, J. E. Lee, J. H. Lee, J. H. Jeong and J. Kim, A biodegradation study of SBA-15 microparticles in simulated body fluid and in vivo, *Langmuir*, 2015, **31**, 6457–6462.

29 J. Kim, W. A. Li, Y. Choi, S. A. Lewin, C. S. Verbeke, G. Dranoff and D. J. Mooney, Injectable, spontaneously assembling, inorganic scaffolds modulate immune cells in vivo and increase vaccine efficacy, *Nat. Biotechnol.*, 2015, **33**, 64–72.

30 C. Lei, P. Liu, B. Chen, Y. Mao, H. Engelmann, Y. Shin, J. Jaffar, I. Hellstrom, J. Liu and K. E. Hellstrom, Local release of highly loaded antibodies from functionalized nanoporous support for cancer immunotherapy, *J. Am. Chem. Soc.*, 2010, **132**, 6906–6907.

31 X. Dong, Z. Wu, X. Li, L. Xiao, M. Yang, Y. Li, J. Duan and Z. Sun, The size-dependent cytotoxicity of amorphous silica nanoparticles: a systematic review of in vitro studies, *Int. J. Nanomed.*, 2020, 9089–9113.

32 O. Gunduz, M. Yetmez, M. Sonmez, M. Georgescu, L. Alexandrescu, A. Ficai, D. Ficai and E. Andronescu, Mesoporous materials used in medicine and environmental applications, *Curr. Top. Med. Chem.*, 2015, **15**, 1501–1515.

33 Y. Li, L. Sun, M. Jin, Z. Du, X. Liu, C. Guo, Y. Li, P. Huang and Z. Sun, Size-dependent cytotoxicity of amorphous silica nanoparticles in human hepatoma HepG2 cells, *Toxicol. In Vitro*, 2011, **25**, 1343–1352.

34 D. Napierska, L. C. Thomassen, V. Rabolli, D. Lison, L. Gonzalez, M. Kirsch-Volders, J. A. Martens and P. Hoet, Size-dependent cytotoxicity of monodisperse silica nanoparticles in human endothelial cells, *Small*, 2009, **5**, 846–853.

35 H. Vallhov, S. Gabrielsson, M. Strømme, A. Scheynius and A. E. Garcia-Bennett, Mesoporous silica particles induce size dependent effects on human dendritic cells, *Nano Lett.*, 2007, **7**, 3576–3582.

36 M. P. Monopoli, C. Aberg, A. Salvati and K. A. Dawson, Biomolecular coronas provide the biological identity of nanosized materials, *Nano-Enabled Med. Appl.*, 2020, 205–229.

37 N. Li, S. Zeng, L. He and W. Zhong, Probing nanoparticle–protein interaction by capillary electrophoresis, *Anal. Chem.*, 2010, **82**, 7460–7466.

38 E. Mahon, A. Salvati, F. B. Bombelli, I. Lynch and K. A. Dawson, Designing the nanoparticle–biomolecule interface for ''targeting and therapeutic delivery'', *J. Controlled Release*, 2012, **161**, 164–174.

39 S. Lara, F. Alnasser, E. Polo, D. Garry, M. C. Lo Giudice, D. R. Hristov, L. Rocks, A. Salvati, Y. Yan and K. A. Dawson, Identification of receptor binding to the biomolecular corona of nanoparticles, *ACS Nano*, 2017, **11**, 1884–1893.

40 A. Lesniak, F. Fenaroli, M. P. Monopoli, C. Åberg, K. A. Dawson and A. Salvati, Effects of the presence or absence of a protein corona on silica nanoparticle uptake and impact on cells, *ACS Nano*, 2012, **6**, 5845–5857.

41 *Guidance on the determination of potential health effects of nanomaterials used in medical devices*, European Commission, 2015.

42 Q. Qian, K. A. Nath, Y. Wu, T. M. Daoud and S. Sethi, Hemolysis and acute kidney failure, *Am. J. Kidney Dis.*, 2010, **56**, 780–784.

43 Y.-S. Lin and C. L. Haynes, Synthesis and characterization of biocompatible and size-tunable multifunctional porous silica nanoparticles, *Chem. Mater.*, 2009, **21**, 3979–3986.

44 K. Stalder and W. Stöber, Haemolytic activity of suspensions of different silica modifications and inert dusts, *Nature*, 1965, **207**, 874–875.

45 E. Casals, T. Pfaller, A. Duschl, G. J. Oostingh and V. Puntes, Time evolution of the nanoparticle protein corona, *ACS Nano*, 2010, **4**, 3623–3632.

46 M. Ahamed, Silica nanoparticles-induced cytotoxicity, oxidative stress and apoptosis in cultured A431 and A549 cells, *Hum. Exp. Toxicol.*, 2013, **32**, 186–195.

47 X. Lu, J. Qian, H. Zhou, Q. Gan, W. Tang, J. Lu, Y. Yuan and C. Liu, In vitro cytotoxicity and induction of apoptosis by silica nanoparticles in human HepG2 hepatoma cells, *Int. J. Nanomed.*, 2011, 1889–1901.

48 O. Tokgun, A. Demiray, B. Kaya, E. R. Karagür, E. Demir, E. Burunkaya and H. Akça, Silica nanoparticles can induce apoptosis via dead receptor and caspase 8 pathway on A549 cells, *Adv. Food Sci.*, 2015, **37**, 65–70.

49 Y. Ye, J. Liu, J. Xu, L. Sun, M. Chen and M. Lan, Nano-SiO2 induces apoptosis via activation of p53 and Bax mediated by oxidative stress in human hepatic cell line, *Toxicol. In Vitro*, 2010, **24**, 751–758.

50 M. Kersting, M. Olejnik, N. Rosenkranz, K. Loza, M. Breisch, A. Rostek, G. Westphal, J. Bünger, N. Ziegler and A. Ludwig, Subtoxic cell responses to silica particles with different size and shape, *Sci. Rep.*, 2020, **10**, 21591.

51 J. Piella, N. G. Bastús and V. Puntes, Size-dependent protein–nanoparticle interactions in citrate-stabilized gold nanoparticles: the emergence of the protein corona, *Bioconjugate Chem.*, 2017, **28**, 88–97.

52 L. Marichal, G. Klein, J. Armengaud, Y. Boulard, S. Chédin, J. Labarre, S. Pin, J.-P. Renault and J.-C. Aude, Protein corona composition of silica nanoparticles in complex media: Nanoparticle size does not matter, *Nanomaterials*, 2020, **10**, 240.

53 T. Yu, A. Malugin and H. Ghandehari, Impact of silica nanoparticle design on cellular toxicity and hemolytic activity, *ACS Nano*, 2011, **5**, 5717–5728.

54 S. Palchetti, L. Digiacomo, D. Pozzi, R. Zenezini Chiozzi, A. L. Capriotti, A. Lagana, R. Coppola, D. Caputo, M. Sharifzadeh and M. Mahmoudi, Effect of glucose on liposome–plasma protein interactions: relevance for the physiological response of clinically approved liposomal formulations, *Adv. Biosyst.*, 2019, **3**, 1800221.

55 S. N. Petrache Voicu, D. Dinu, C. Sima, A. Hermenean, A. Ardelean, E. Codrici, M. S. Stan, O. Zărnescu and A. Dinischiotu, Silica nanoparticles induce oxidative stress and autophagy but not apoptosis in the MRC-5 cell line, *Int. J. Mol. Sci.*, 2015, **16**, 29398–29416.

56 M. S. Stan, I. Memet, C. Sima, T. Popescu, V. S. Teodorescu, A. Hermenean and A. Dinischiotu, Si/SiO_2 quantum dots cause cytotoxicity in lung cells through redox homeostasis imbalance, *Chem.-Biol. Interact.*, 2014, **220**, 102–115.

57 S. Hussain, K. Hess, J. Gearhart, K. Geiss and J. Schlager, In vitro toxicity of nanoparticles in BRL 3A rat liver cells, *Toxicol. In Vitro*, 2005, **19**, 975–983.

58 G. Parsonage, A. D. Filer, O. Haworth, G. B. Nash, G. E. Rainger, M. Salmon and C. D. Buckley, A stromal address code defined by fibroblasts, *Trends Immunol.*, 2005, **26**, 150–156.

59 RheoSense, Viscosity of Fetal Bovine Serum and Media Formulations, *https://www.rheosense.com/ cell-tissue-culture-media*, 2020.

60 RheoSense, Viscosity of DMEM Cell Culture Media, *https://www.rheosense.com/ dmem-cell-culture-media*, 2020.

61 M. P. Monopoli, A. S. Pitek, I. Lynch and K. A. Dawson, Formation and characterization of the nanoparticle–protein corona, *Nanomaterial Interfaces in Biology: Methods and Protocols*, 2013, pp. 137–155.

62 K. Partikel, R. Korte, N. C. Stein, D. Mulac, F. C. Herrmann, H.-U. Humpf and K. Langer, Effect of nanoparticle size and PEGylation on the protein corona of PLGA nanoparticles, *Eur. J. Pharm. Biopharm.*, 2019, **141**, 70–80.

63 M. M. Bradford, A rapid and sensitive method for the quantitation of microgram quantities of protein utilizing the principle of protein-dye binding, *Anal. Biochem.*, 1976, **72**, 248–254.

64 H. Zhang, D. R. Dunphy, X. Jiang, H. Meng, B. Sun, D. Tarn, M. Xue, X. Wang, S. Lin and Z. Ji, Processing pathway dependence of amorphous silica nanoparticle toxicity: colloidal vs pyrolytic, *J. Am. Chem. Soc.*, 2012, **134**, 15790–15804.